doi:10.1038/nature12342

Sample description and geologic background

The 1963-65 Irazú eruption is dominated by shallow crustal mixing and hybridisation, which has almost completely obscured the mixing end-member magma compositions[11]. The phenocryst assemblage is dominated by shallow crystallisation from this hybrid melt (i.e., zoned plagioclase, multiple populations of clinopyroxenes, olivines overgrown by orthopyroxenes), yet rare magnesian olivines (~ 2 vol.% of the total magma) are present. Of these 2 vol.% about every tenth records significant Ni reversal. Thus, despite this compositional blending some magnesian olivine phenocrysts keep a record of variable mantle-melt compositions.

Samples from 1963-65 crater rim deposits on the SW side of the major Irazú crater[15] were collected in 2010. IZ-10-13 and IZ-10-11 were collected ~ 1.2 m apart from each other above and below a prominent package of juvenile scoria-rich tephra in the middle of the rim deposits of the 1963-65 eruption (Fig. S1). Assuming linear deposition, they span between 6-9 months of eruptive activity, where IZ-10-13 is stratigraphically on top and erupted later. Samples taken from ash to fine lapilli layers ensure rapid cooling upon fragmentation and limited post-eruptive overprinting by slow cooling[43]. Random olivine phenocrysts were hand-picked from sieved (125-250 µm, 250-500 µm, 500-1000 µm) tephra. They were cleaned in an ultrasonic bath and mounted as randomly oriented grains. Grains were exposed and polished for imaging via electron microprobe. This imaging guided our LA-ICPMS analysis. Pictures were taken to locate precisely the laser track (Fig. S6 and S7). After removing the laser track and repolishing the olivine grains, grain orientations were determined via electron-backscattered diffraction. At this stage we also analysed exposed melt inclusions (Tab. S2) to supplement existing data[22].

Magnesian olivines with large Ni variations – a discussion of their origin

To use magnesian olivines with Ni zonation as recorders for Moho-to-surface ascent timescales requires that (1) the crystals are in fact carried by magma from near-Moho depth to the surface and (2) the initial step-wise Ni zonation is generated by mixing of two primary melts with distinct Ni activities (but similar Fe/Mg ratio) prior to

magma ascent from the Moho. Below we argue why these assumptions are met and why most alternative mechanisms for erupting magnesian olivines with Ni zonations fail in either (a) preserving or generating magnesian olivines and/or (b) recording Ni variations that persist until the crystals get quenched after eruption. While it may be possible for primary magmas to mix in the crust, dike transport calculations show that this process requires even faster ascent than the more conservative mantle-mixing scenarios favored here. Thus, rapid (< 1 year) transport is an inevitable requirement of Ni zonation in the magnesian cores of olivines.

Possibility 1) The magnesian olivines are not true phenocrysts (i.e. growth from a magmatic liquid) but instead are zoned xenocrysts (i.e. foreign crystals that the magma picked up along the way) either assimilated in the mantle or from crustal wall rocks

Let us first point out that even if Irazu magnesian olivines are ***mantle*** xenocrysts, the Ni zonation in their interiors still constrains the timescale of ascent from the mantle. The actual origin of these olivines in the mantle is largely immaterial to their use as a chronometer for mantle-to-surface transport. Even so, there are several arguments against the Irazú magnesian olivines being mantle xenocrysts. Mantle xenocrysts and xenoliths typically show a narrow compositional range in major and trace elements due to their long residence times (millions of years) at high temperatures (> 1200 ˚C) in the mantle; e.g., any Ni zonation is completely erased within a few hundred years ($t \sim 200$ yr with $t \sim x^2/D$, assuming D along [001] at 1200 ˚C and $x = 500$ μm). While rims in mantle xenocrysts may vary as a result of recent melting or fluid-rock interaction[44], olivine cores are generally uniform. This is inconsistent with the large compositional variations found in the magnesian (> Fo_{88}) cores of Irazu olivines, which show a large range in both major (Fo_{88-91}) and trace elements (Ni varying ~ 1500 pm at constant Fo; Fig. S2). Low CaO concentrations in olivines similar to the ones found in Irazú olivines (grey and blue symbols in Fig. S2) have been traditionally interpreted as mantle xenocrysts[45]. However, recent studies[46,47] have shown that low-CaO olivines may respresent phenocrysts that crystallise from low-CaO magmas, like those common to Irazú (near the low end of the global spectrum[48]). Lastly, mantle xenoliths are typically coarse-grained (> 1000 μm)

with anhedral crystals, while most magnesian olivines in Irazú tephra are small (< 500 μm) and euhedral (i.e., well-formed crystals are testimony to free growth from liquid).

The same textural arguments also apply to ***crustal*** xenocrysts derived from magmatic ultramafic cumulates. Here, additional compositional and thermal constraints make it even more difficult to preserve magnesian olivines. First, unless interstitial melt is completely expelled during olivine cumulate formation, the subsolidus cooling and complete crystallization causes reequilibration of the major elements to lower Fo olivine[49]. Indeed, olivine-bearing crustal cumulates typically contain olivines with intermediate Fo[24,50] (Fo_{70-85}) and therefore do not resemble the magnesian Irazú olivine phenocrysts. In fact, such intermediate olivine crystals exist also at Irazú and are easily recognized by their distinct trace element compositions (Fig. S2) and often anhedral appearance with occasional pyroxene overgrowth. These olivine xenocrysts (mantle or crustal origin; brown and black symbols in Fig. S2) show anomalous high Co/Mn (i.e., inconsistent with primarily olivine fractionation) for their respective Fo content, and one of those xenocrystic populations (brown) has also distinctively low CaO contents. In addition to the intermediate composition of crustal xenocrysts, prolonged elevated temperatures in mush systems would lead to enhanced diffusive re-equilibration of not just major elements, but also trace elements such as Ni. Thus, even if magnesian olivines are preserved by efficient olivine-melt separation, Ni reversals would not be preserved (or at least significantly relaxed) as cooling and arresting diffusive reequilibration would not be fast enough in areas of elevated geotherms such as active, mature volcanic arcs[2] like Central America.

Thus, a combination of thermal, compositional, and textural arguments does not support a xenocrystic origin for the magnesian olivines in Irazú tephra, but instead an origin initially as phenocrysts in primitive mantle melts that later hybridize at shallow levels.

Possibility 2) The magnesian olivines crystallized at shallow depth and therefore would have no bearing on Moho-to-surface ascent rates

Olivine is typically recognized as a shallow liquidus phase, particularly in dry, tholeiitic melts[21]. At greater depth olivine may be replaced by pyroxene as the first

silicate phase on the liquidus. Thus, one could argue that if olivine is the liquidus phase (which is supported by the fact that olivines have the highest Mg numbers ($Mg^{2+}/(Mg^{2+}+Fe^{2+})$ on an atomic basis) primitive melts are aphryic (free of crystals) for most of their ascent, and only when they reach the water-saturated solidus, olivine crystallisation commences[2]. However, for such a scenario to generate magnesian olivines with internal Ni zonation requires the mixing of two primitive melts at shallow levels where one or both melts contain magnesian crystallites (< 200 μm) prior to the mixing. Under this scenario (1) primitive melts cannot homogenize prior to some olivine growth (otherwise Ni zonation would not be generated) and (2) primitive melts cannot cool and fractionate on their way to shallow levels or mix with more evolved magmas during ascent (otherwise Fe/Mg ratios would be too high for $Fo_{>88}$ to crystallise). We consider the latter requirement below, in a dike transport calculation, to demonstrate that this scenario requires even more rapid ascent times than the mantle-to-surface ones we favor. Moreover, geophysical studies have identified a shallow magma storage region at 5-10 km depth beneath Irazú[12,28]. Given that erupted magmas are typically hybrid andesites[11] it seems reasonable that hybridization happens at this level, and so magnesian olivine growth and mixing of primitive melts likely occur at greater depth - at least at mid to lower crustal levels.

Possibility 3) The magnesian olivines crystallized at mid to lower crustal levels and therefore would have little bearing on Moho-to-surface ascent rates

Arc magma systems are envisioned to encompass polybaric storage regions in the crust[2,51], which may include significant melt pockets at mid and lower crustal levels. In this case, olivine crystallisation and mixing of primitive melts may occur not at near-Moho depths, but at intermittent regions of magma accumulation. While such crustal "hot zones" may be excellent sites for magma differentiation, they are not favorable to the preservation of magnesian olivines. An extensive lower crustal storage zone of mantle-derived melts will be characterized by (1) elevated geotherms (~ 1000 ˚C) throughout most of the lower crust and (2) a significant amount of intermediate melt present[2]. Newly arriving primitive aphyric magmas would mix with the intermediate composition magmas, lowering their Mg/Fe ratio, and thereby losing their capability to crystallise high

Fo olivines. If the newly arriving magmas were already partially crystallised (i.e. containing high Fo olivines), mixing with intermediate magmas and continued crystallisation would produce Ni variations that would not follow the predominantely olivine-only fractionation trends observed in Irazú olivines (Fig. S2). Thus, any lower crustal hot zone would preclude mixing of primitive mantle melts as those melts would not retain their high Mg/Fe character[52]. In an opposite case, where the lower crust has not been heated due to magma input and storage to 1000 ˚C, more modest geotherms put lower crustal temperatures between 500 to 700 ˚C[52]. Under such conditions a hot primitive magma will rapidly fractionate to more intermediate compositions[52], and subsequent mixing with a second primitive magma will not produce unzoned, high-Fo magnesian olivines as observed.

In summary, the arguments presented above provide constraints on the magnesian olivine crystals: these crystals are phenocrysts that grew from primitive mantle melts below the Moho, where high Mg/Fe ratios can persist over extended times. Recent experimental studies confirm that hydrous arc basalts may crystallise olivine as the first silicate phase[27] even at Moho pressures (~ 1 GPa). Furthermore, if olivine growth occurs at Moho depth, Ni zonation provides evidence for mixing of distinct mantle melts at that depth, and the crystals record timescales for Moho-to-surface ascent.

Thermal considerations on dike propagation

The thermal requirements of magma transport in dikes can be used to test two scenarios of magma mixing and ascent. The first is the case presented in the main text of the paper, whereby magnesian olivines (> Fo_{88}) acquire their Ni zonation profiles in the mantle, and the diffusive timescales we calculate (~ 1 year; Fig. 4) relate to mantle-to-surface ascent that occurs on the order of 50-100 m/day. The thermal requirement of this scenario is that this magma, which represents the recharge mass and heat of the erupted system, arrives at the shallow magma chamber at a temperature higher than the ~1050°C estimated from whole rock samples and melt inclusion data of more evolved compositions[22] for the hybrid magma that erupts. We take this temperature of the recharge magma to be at least 1100˚C, given calculated melt-olivine temperatures for the 1963-65 eruption (Table S2). Assuming conservative estimates (2-4 wt.% H_2O) for water

in the melt and using the thermometer of ref. 55,56 together with the hydrous liquid depression in ref. 54 we obtain the temperature range (1100-1200˚C) used in our diffusion modeling calculations. Other thermodynamic models[21,25] confirm this temperature range for wet primitive magma compositions at Irazú. Thus, dike transport must be efficient enough so that the magma does not cool below this temperature. The second case is Possibility 2 above, where magma mixing of distinct mantle melts occurs in the shallow crust. The thermal requirement of this scenario is more stringent that magnesian olivines remain unzoned (as observed). For this to happen, dike transport must be efficient enough that magma cools less than 35°C (equivalent to 1 Fo unit[21]).

We explore these two cases by employing a simple finite-volume advection-diffusion model to calculate the temperature distribution for a dike of half width w, length h (where $h \gg w$; and in the calculations $h = z$, with z = 30 km), and magma ascent velocity u (100 m/day) solving the steady-state equation for advective-conductive heat transfer :

$$\rho u \frac{\partial T}{\partial z} = \frac{\kappa}{c_p} \nabla^2 T \qquad \text{(eq. S1)}$$

with ρ, κ, and c_p being the the magma density (2800 kg m^{-3}), the thermal conductiviy (κ = 2.0 W(mK)$^{-1}$) and the heat capacity, respectively. The heat capacity term in equation S1 includes latent heat (500 kJ/kg), as we combine the heat capacity (1.0 kJ(kgK)$^{-1}$) with a latent heat term in which a linear melt fraction variation between a solidus (800 ˚C) and liquidus (1200 ˚C) is assumed that adds an additonal 1.25 kJ(kgK)$^{-1}$ to the heat capacity term. By solving the steady-state heat equation (eq. S1) we obtain the most favorable condition for minimal cooling in the dike. To further simplify the problem, we consider a constant temperature distribution T_∞ in the wall rocks beyond a boundary layer of constant thickness. Two wall rock temperature models $T_\infty(z)$ are considered: Model 1 with a linear geotherm from 1000°C at the Moho to 800°C at the surface is motivated by thermal models[2] that suggest that the deep crust may be a zone of magma accumulation and differentiation through extensive sill injection, and Model 2 with a constant-temperature crust of 800 °C is motivated to minimise melting of wall rocks (Fig. S3c). In

both models upper crustal temperatures are much higher than normal geotherms given that Irazú volcano has been a locus of volcanic activity for several 100 kyr[11] and sustains an upper crustal magma chamber[12,28]. Moreover, we also consider two boundary layer thicknesses w_{BL} ($w_{BL} \sim \sqrt{(kt)}$ with the thermal diffusivity $k = \kappa (\rho c_p)^{-1}$), which heat up during magma transport: one consistent with a thermal aureole developed over one week of magma transport (w_{BL} = 0.44 m) and the other over one year (w_{BL} = 3.2 m). As expected, magma cools the least for dikes of greatest width (6-8 m), for the Model 1 geotherm (the warmer of the two), and the widest boundary layer between the dike and wallrocks (panel b). For simplicity the same physical parameters are used to describe heating and melting in the country rock boundary layer. The inflowing magma at the base of the dike in these models is taken to be 1200 ˚C. A more detailed discussion of this model will be presented elsewhere. Thermal effects due to adiabatic ascent (i.e. intrinsic cooling of these ascending magmas due to volume increase) are not included.

The results of the dike model can be used to test the two cases outlined above. In the first case, mafic magmas will retain enough heat (> 1100 ˚C) in the shallow crust only if dike widths are large (6-8 m). Regional studies of dike width distributions show that post-emplacement dike width is often < 2 m[53], and if this were a true limit, then it would require even faster magma ascent than the conservative ones calculated from the Ni profiles (100 m/day). A 2 m dike with the most favorable wall rock thermal profile (Model 1 and widest w_{BL}) would require ~ 400 m/day ascent rates to remain above 1100˚C at 25 km, the distance between the Moho and the shallow magma chamber. Magmas could stall for a period of time beneath the Moho after mixing, experiencing minimal heat loss to the mantle surroundings, and then rise at a faster rate than the average calculated here from the total distance (30 km) and total time (~ 300 days). Thus, thermal considerations point to even faster ascent rates from the Moho to the surface than the minimum ascent rates calculated for Ni in Irazu olivines.

In the second case, none of the transport models are efficient enough to prevent significant cooling, which would create zoned and lower Fo olivine crystals prior to mixing in the shallow crust. Near-adiabatic conditions are required to minimise cooling to less than 35°C (< 1 Fo unit), and this in turn requires at least one order of magnitude faster average ascent rates (Fig. S3). Distinct magmas would have to transit from the

mantle to the crust in less than a month (25 days @ 1000 m/day) in short succession. Thus, in this scenario, magmas would have to ascend even faster through the crust than in the case where primitive magmas mix in the mantle.

As shown in these thermal models, the competition between ascent and crystallisation is very sensitive. The calculations demonstrate that (1) the timescales inferred from Ni zonation are consistent with thermal requirements, given efficient dike transport in wide dikes (6-8 m), and (2) scenarios whereby magmas retain their mantle temperatures and composition prior to mixing in the upper crust require one order of magnitude faster transport. Thus, the combined constraints on timescales provided by both chemical zonation and thermal evolution inevitably point to magma ascent from Moho to surface that is fast, < 1 year, and > 100 m/day. The most likely scenario is that Irazú olivines crystallised deep, presumably close to the Moho as the distinct primitive magmas pool and mix at the rheological discontinuity. Rapid ascent is then required to prevent cooling and fractional crystallisation, which would generate lower magnesian olivines and greater zonation in major elements than is observed at Irazú.

Comparison of electron microprobe and laser ablation-ICPMS profiles

We have tested if laser data are strongly affected by smearing from the large laser spot and the prolonged transport of the ablated material from the sample cell to the torch. Fig. S4 shows a comparison of a laser traverse with a microprobe traverse for three crystals. The microprobe traverse was taken along the same traverse after polishing down the previous laser track. LA-ICPMS traverse zoning is comparable to the zoning documented via microprobe spot analyses. Both the amplitude and the wavelength of Ni (and for that matter also Cr) variations are almost identical when measured by these two techniques, suggesting that LA-ICPMS profiles resolve gradual variations, and that the inevitable smearing of sharp step variations is insignificant for our analysis. Therefore, maximum timescale estimates are not controlled by the smearing of the laser signal and instead are reasonable maximum timescales for Ni reversals in the Irazú olivines.

Crystal fractionation based on other elements

A total of 40 crystal traverses show compositional variations in other trace elements consistent with olivine-dominated fractional crystallisation recorded in primitive olivines (> Fo_{88} and > 1500 ppm Ni, Fig. S5). Incompatible element concentrations in olivine (Ca, Ti, Sc) increase as melt compositions become enriched in these elements. Although more traverses probably follow this simple fractionation trend, we have screened the dataset for traverses that have good data quality for trace elements and have only limited contamination by Cr-spinel inclusions. A few crystal traverses that record more evolved melt compositions indicate plagioclase crystallisation (steady CaO at low Ni) and additional crystallisation of pyroxenes (kink at ~ 1500 ppm in Ti and Sc).

References (SM)

43. Lloyd, A., Plank, T., Ruprecht, P., Hauri, E. & Rose, W. Volatile Loss from Melt Inclusions in Pyroclasts of Differing Sizes. *Contributions to Mineralogy and Petrology* ((in press)).doi:10.1007/s00410-012-0800-2
44. Kelemen, P.B. Genesis of high Mg# andesites and the continental crust. *Contr. Mineral. and Petrol.* **120**, 1–19 (1995).
45. Simkin, T. & Smith, J.V. Minor-Element Distribution in Olivine. *The Journal of Geology* **78**, 304–325 (1970).
46. Kamenetsky, V.S., Elburg, M., Arculus, R. & Thomas, R. Magmatic origin of low-Ca olivine in subduction-related magmas: Co-existence of contrasting magmas. *Chemical Geology* **233**, 346–357 (2006).
47. Elburg, M., Kamenetsky, V.S., Nikogosian, I., Foden, J. & Sobolev, A.V. Coexisting high- and low-calcium melts identified by mineral and melt inclusion studies of a subduction-influenced syn-collisional magma from South Sulawesi, Indonesia. *Journal of Petrology* **47**, 2433–2462 (2006).
48. Plank, T. & Langmuir, C.H. An evaluation of the global variations in the major element chemistry of arc basalts. *Earth and Planetary Science Letters* **90**, 349–370 (1988).
49. Barnes, S.J. The effect of trapped liquid crystallization on cumulus mineral compositions in layered intrusions. *Contributions to Mineralogy and Petrology* **93**, 524–531 (1986).
50. Otamendi, J.E., Cristofolini, E., Tibaldi, A.M., Quevedo, F.I. & Baliani, I. Petrology of mafic and ultramafic layered rocks from the Jaboncillo Valley, Sierra de Valle Fértil, Argentina: Implications for the evolution of magmas in the lower crust of the Famatinian arc. *Journal of South American Earth Sciences* **29**, 685–704 (2010).
51. Ruprecht, P., Bergantz, G.W., Cooper, K.M. & Hildreth, W. The crustal magma storage system of Volcán Quizapu, Chile, and the effects of magma mixing on magma diversity. *Journal of Petrology* **53**, 801–840 (2012).

52. Dufek, J. & Bergantz, G.W. Lower Crustal Magma Genesis and Preservation: a Stochastic Framework for the Evaluation of Basalt-Crust Interaction. *J. Petrology* **46**, 2167 – 2195 (2005).
53. Walker, G.P.L., Eyre, P.R., Spengler, S.R., Knight, M.D. & Kennedy, K. Congruent dyke-widths in large basaltic volcanoes. *Physics and Chemistry of Dykes* 35–40
54. Médard, E., and Grove, T.L., 2008, The effect of H2O on the olivine liquidus of basaltic melts: experiments and thermodynamic models: Contributions to Mineralogy and Petrology, v. 155, no. 4, p. 417–432.
55. Putirka, K.D., 2008, Thermometers and barometers for volcanic systems: Reviews in Mineralogy and Geochemistry, v. 69, no. 1, p. 61–120.
56. Sugawara, T., 2000, Empirical relationships between temperature, pressure, and MgO content in olivine and pyroxene saturated liquid: Journal of Geophysical Research, v. 105, no. B4, p. 8457–8472.

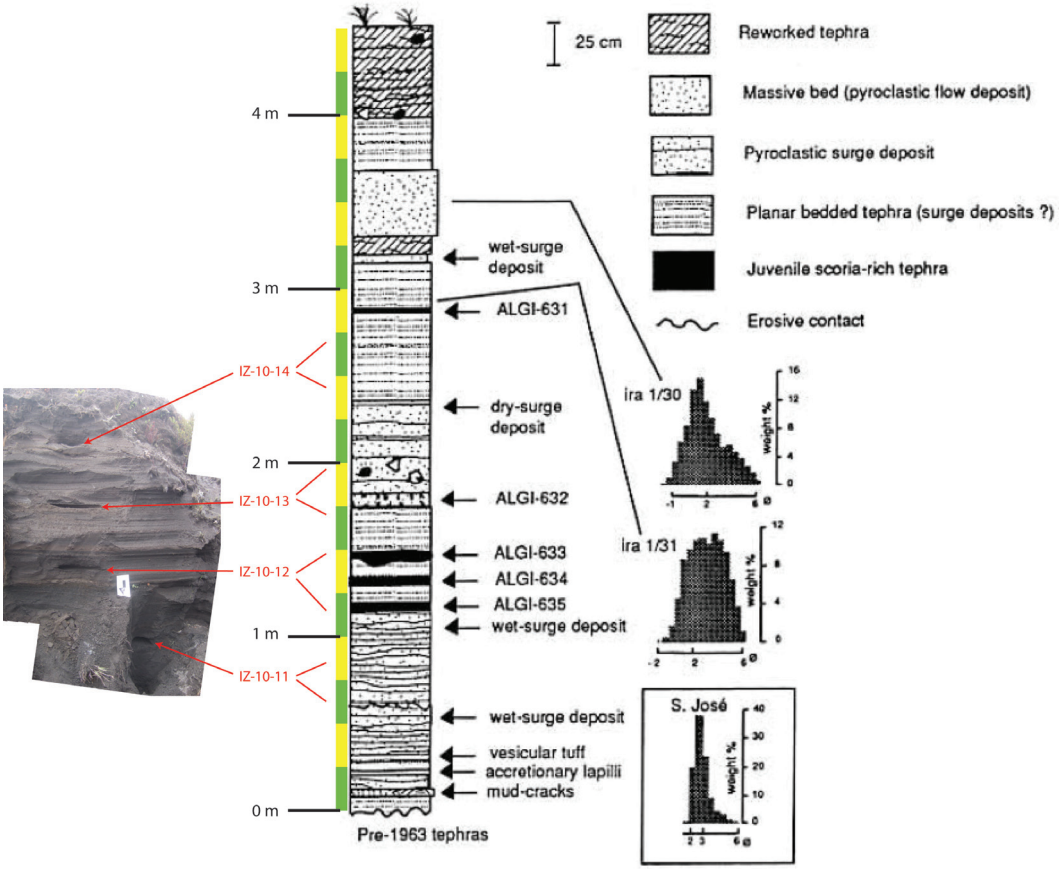

Figure S1. Approximate correlation of sample locations with the composite stratigraphic column (Fig. 13 of Ref. 15) of the 1963-1965 Irazú eruption. Assuming constant deposition rate throughout the two years of eruption suggests that samples IZ-10-13 and IZ-10-11 span 6-9 months of the eruptive episode.

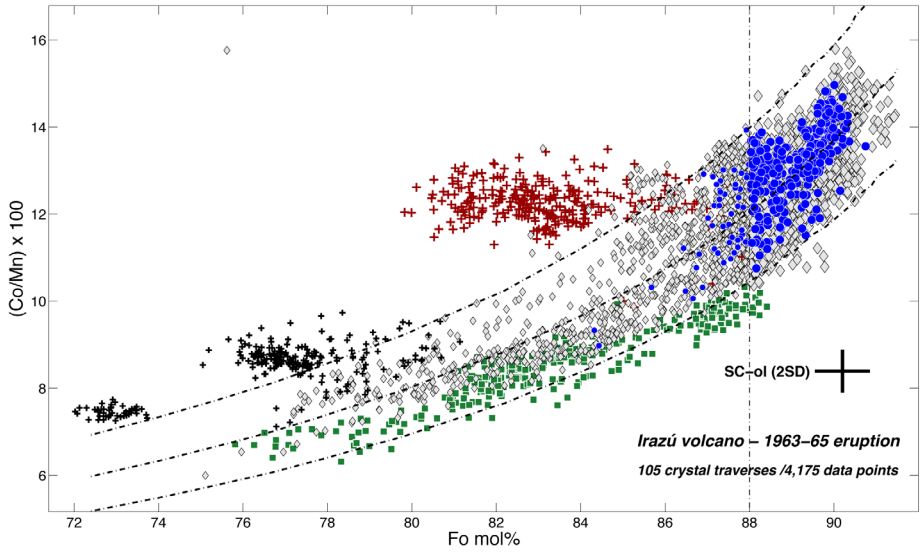
(Co/Mn) x 100
Fo mol%
SC–ol (2SD)
Irazú volcano – 1963–65 eruption
105 crystal traverses /4,175 data points

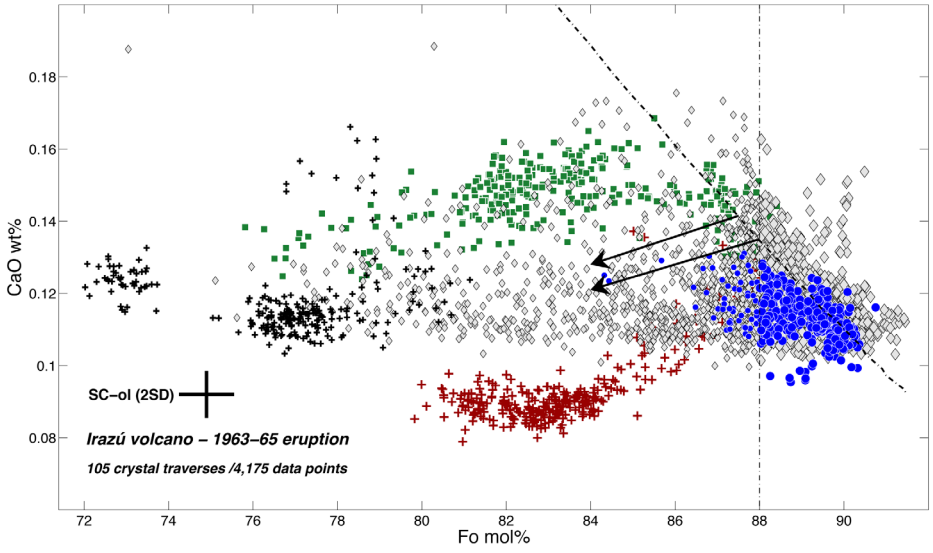
CaO wt%
Fo mol%
SC–ol (2SD)
Irazú volcano – 1963–65 eruption
105 crystal traverses /4,175 data points

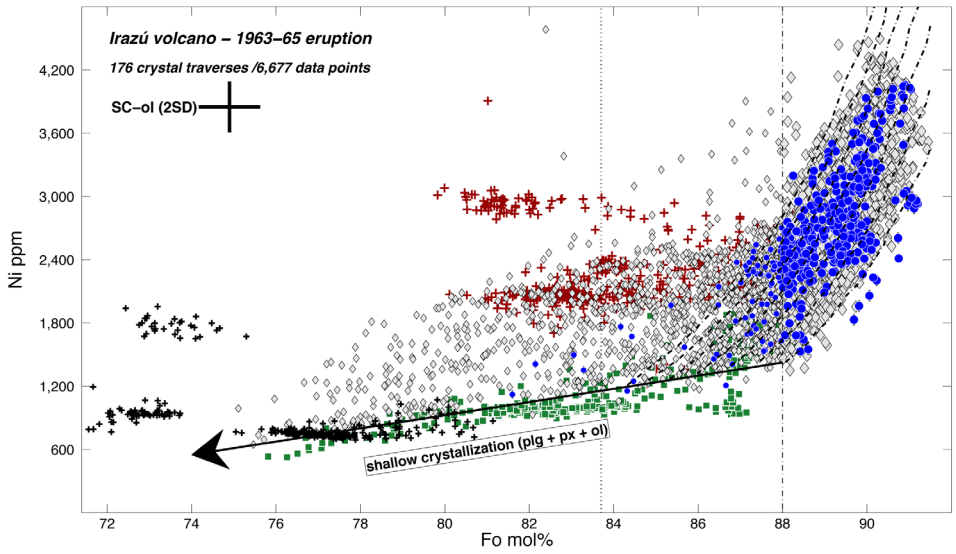
Irazú volcano – 1963–65 eruption
176 crystal traverses /6,677 data points
SC–ol (2SD)
Ni ppm
Fo mol%
shallow crystallization (plg + px + ol)

Figure S2. (a) Co/Mn, (b) CaO, and (c) Ni versus forsterite content (Fo) measured by laser-ablation ICPMS for a subset of samples from Fig. 1. Colors refer to different olivine populations distinguished compositionally and texturally. Olivine phenocrysts that are used for Ni diffusion timescale calculations (blue) are highlighted from other phenocrysts (grey) to show that they respresent the common compositional variability in the high Fo Irazú olivines. Xenocrysts (low Fo content: black +; intermediate Fo, low Ca: brown +) form distinct clusters in many variation diagrams and deviate from olivine fractionation control lines. An additional end-member population of normally zoned (decreasing Fo content from crystal core to rim) olivines (green squares) with broad Fe-Mg zones is overall similar to Irazú olivine phenocrysts, but represents an end-member trend in the intermediate Fo olivines (highest CaO, lowest Co/Mn, lowest Ni). The broad zonations suggest prolonged storage in the magma system and partial equilibration in a more evolved melt of these so-called antecrysts. (a) Olivine fractionation curves (dashed, calculated using Beattie et al. 1991) for a high- and low-Co-Mn olivine-only fractionation trend assume 35.9 ppm Co and 0.093 wt.% MnO at 8.08 wt.% MgO and 30.6 ppm and 0.082 wt.% at 9.53 wt.% MgO, respectively. Olivine-only fractionation is limited mainly to > Fo_{88} (thin dash line). (b) Olivine fractionation curves (dashed, calculated using Beattie et al. 1991) assume 2.2 wt.% CaO at 8.08 wt.% MgO, respectively. The pair of arrows shows qualitatively the trend of additional plagioclase and clinopyroxene crystallization. (c) Curves as in Fig. 1.

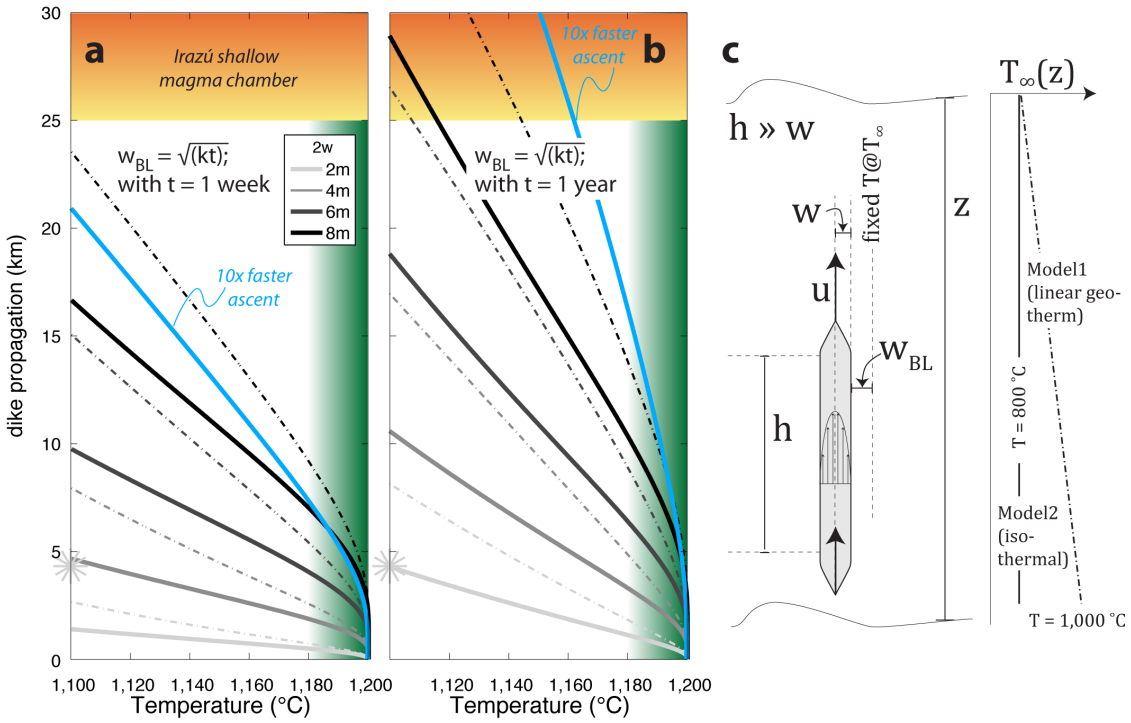

Figure S3. Temperature distribution along the center of a simplified dike. Laminar flow with no-slip boundaries is assumed across the width of the dike with an average velocity of u = 100 m/day allowing horizontal heat flow only by diffusion. A fixed far-field temperature $T_\infty(z)$ (Dash-dot curves: Model 1; Solid bold curves: Model 2) at distance w_{BL} leads to heat loss during dike ascent. Two different boundary layer thicknesses w_{BL} are used given heat transfer affecting the country rock continuously for one week (a) and one year (b), respectively (see text for explanation). The Irazú shallow magma chamber ~ 25 km (yellow-red field) above the Moho represents an area were any mafic magma would lose its primitive character through magma mixing. Near-adiabatic ascent (< 20 ˚C cooling which is the common uncertainty for temperature determinations; green field) requires at least one order of magnitude faster ascent rates (blue curves are for 1000 m/day and a 2 m wide dike).

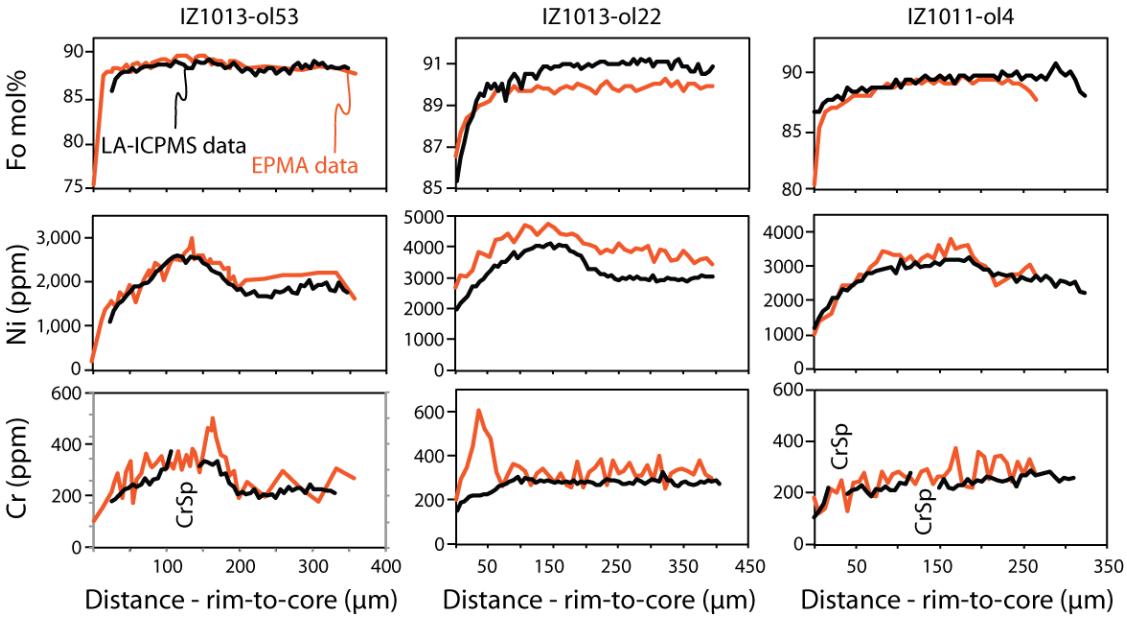

Figure S4. Comparison of microprobe and laser-ablation ICPMS traverses for three crystals. Measurements along the EPMA traverses were taken along the same path as the LA-ICPMS traverses, however after polishing down into the grain additional 60 µm to remove the laser track. There is good agreement between EPMA and LA-ICPMS data with respect to spatial resolution and concentration for Fo, Ni, and Cr. Only IZ1013-ol22 shows significant variations in the absolute values of Fe/Mg ratio and Ni concentrations pointing to either uncertainties in the calibration or to significant variations during depth profiling. Large Cr concentrations are the result of partial ablation of Cr-rich spinels.

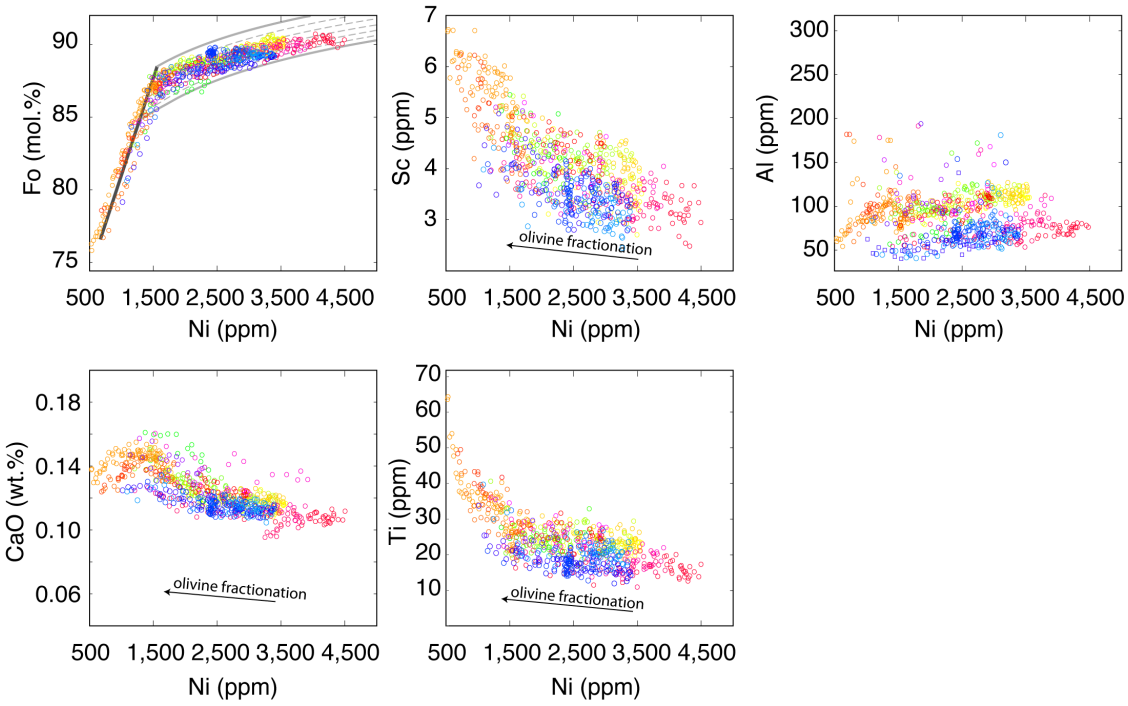

Figure S5. Trace element variations as a function of Ni content for 24 olivines (out of the 176 olivines analysed) that most closely follow simple olivine fractionation. Olivine fractionation arrow assumes perfect incompatibility for Ca, Ti, and Sc over the observed compositional range of primitive olivine (Fo_{88-91}). Symbol colours vary for each crystal.

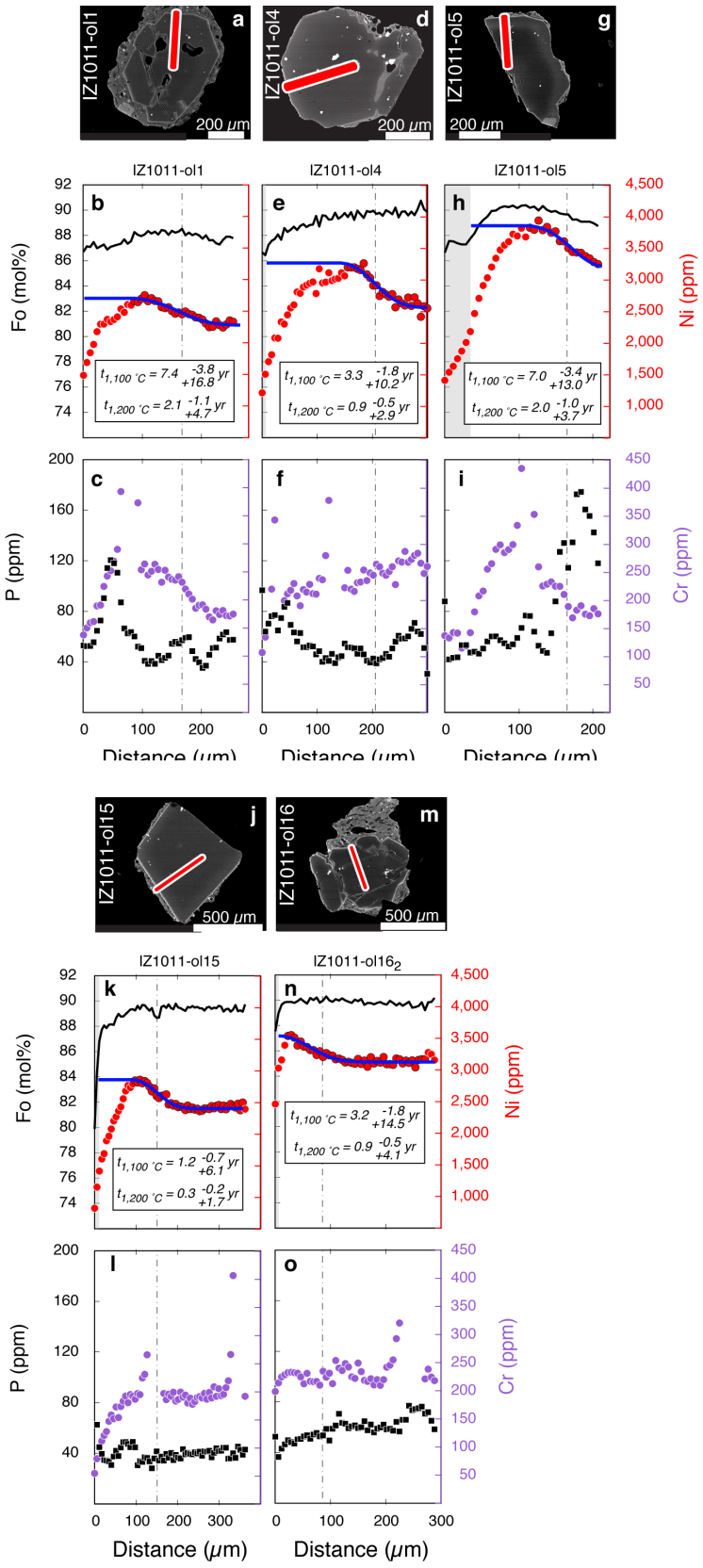

Figure S6. Compilation of olivine phenocrysts from IZ-10-11 for which mixing timescales via Ni zonation were calculated. Top row: Back-scattered electron images

highlighting the minimal zonation of major elements in the interior of the olivines. Lighter rims are Fe-rich olivine and white inclusions are Cr-spinels. Bold red line shows the location of the LA-ICPMS raster path. Middle row: Fo (black line) and Ni (red circles) zonation calculated from LA-ICPMS traverses with distance measured from the rim. Shown are the best-fit diffusion profiles (blue curves). The mixing-to-eruption timescales represent the mode of the probability density functions (PDFs) derived via a Monte-Carlo approach. Note that the best-fit diffusion profiles are in a some cases calculated for timescales that differ from the mode of the PDFs. Bottom row: Zoning of slow diffusing elements (phosphorous: black; chromium: purple). Grey bars indentify the part of the crystals that was not modeled, as this part likely crystallised late during decompression and degassing (see also Fig. S8).

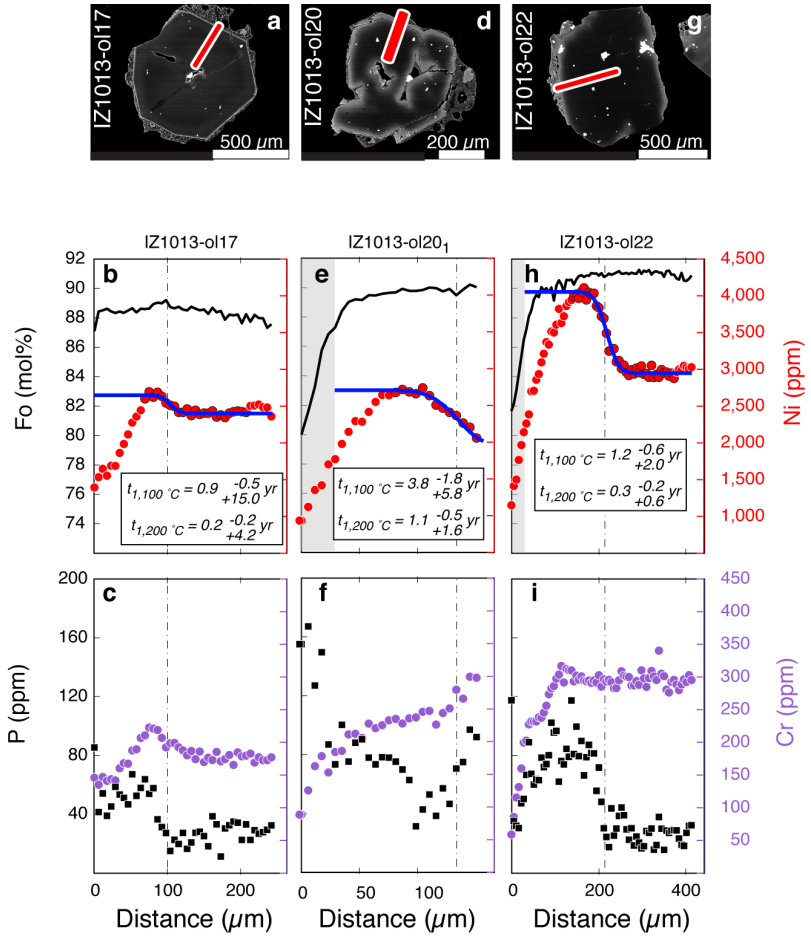

Figure S7. Compilation of olivine phenocrysts from IZ-10-13 for which mixing timescales via Ni zonation were calculated. Symbols as in Fig. S6.

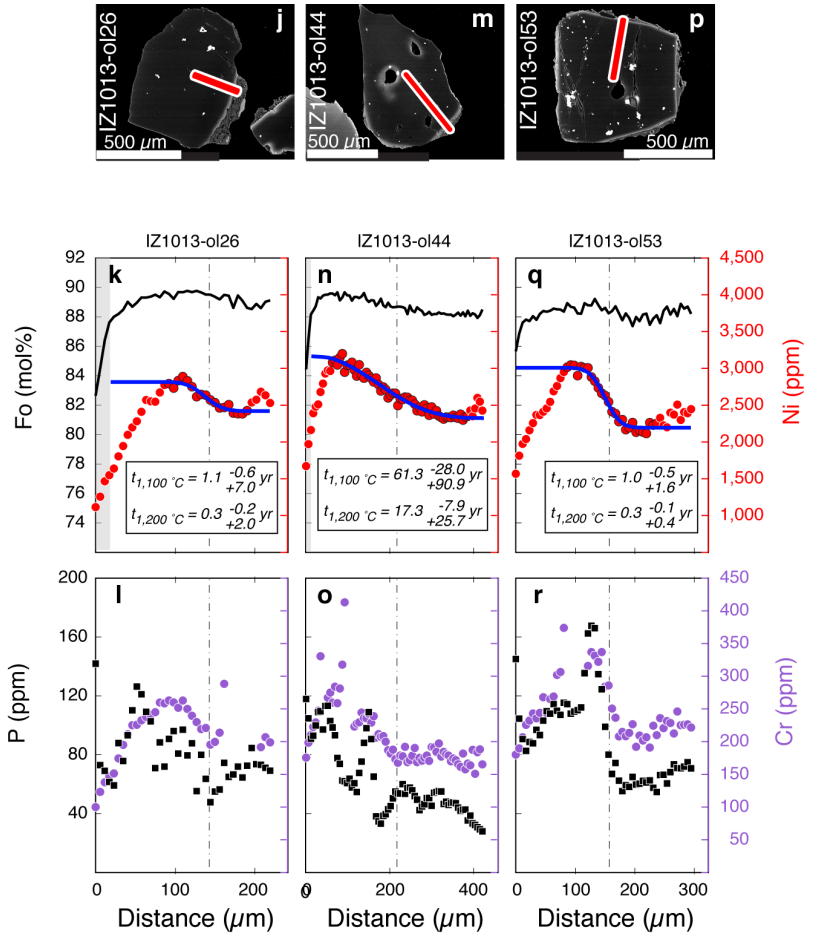

Figure S7. Continued.

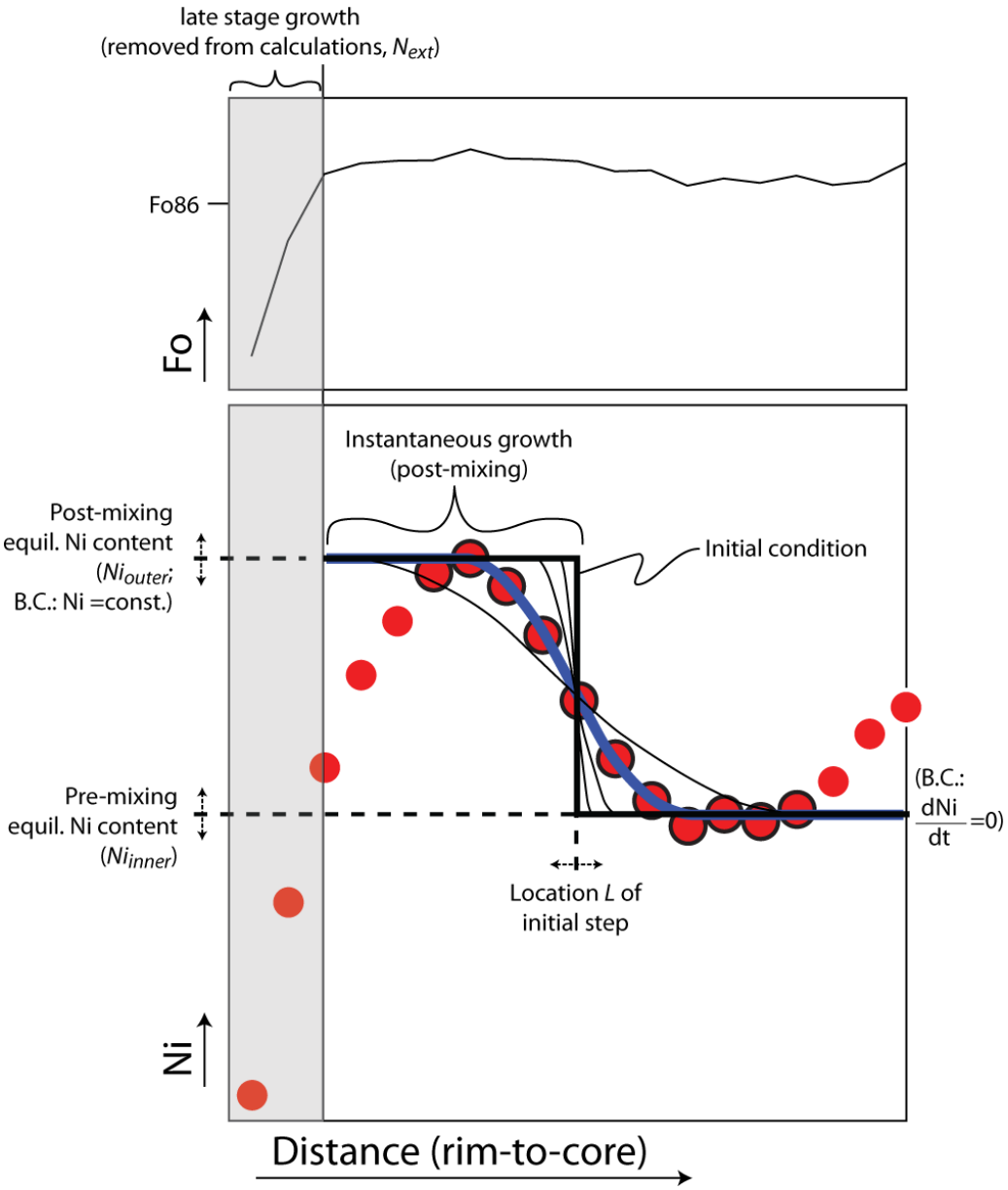

Figure S8. Schematic showing the initial and boundary conditions (B.C.) used for each diffusion calculation. Root-mean squares (RMS) between model (curved lines) and data defining the reverse step (black-rimmed red circles; N_{RMS} in Tab. S4) were calculated to estimate the best fit time scales (blue line). White-rimmed red data points are not used to calculate the RMS, because we wish to isolate the reversal step in the diffusion modeling. Dashed arrows indicate parameters that were varied to optimise the fit. Rim compositions below Fo_{86} were removed for the calculations. In addition to the variables illustrated, we also choose a range of angles between diffusion direction and lattice orientation.